Journal of Advanced Research (2017) 8, 279–288

Cairo University

Journal of Advanced Research

ORIGINAL ARTICLE

Effective role of CaO/P_2O_5 ratio on SiO_2-CaO-P_2O_5 glass system

P. Kiran [a,*], V. Ramakrishna [b], M. Trebbin [b], N.K. Udayashankar [a], H.D. Shashikala [a]

[a] Department of Physics, Crystal Growth Laboratory, National Institute of Technology Karnataka, Surathkal 575025, India
[b] Hamburg Center for Ultrafast Imaging (CUI), University of Hamburg, Luruper Chaussee 149, 22761 Hamburg, Germany

GRAPHICAL ABSTRACT

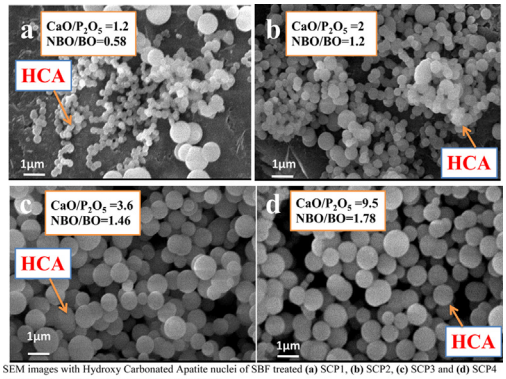

SEM images with Hydroxy Carbonated Apatite nuclei of SBF treated **(a)** SCP1, **(b)** SCP2, **(c)** SCP3 and **(d)** SCP4 glasses with CaO/P_2O_5 co-related to NBO/BO ratio.

ARTICLE INFO

Article history:
Received 21 December 2016
Received in revised form 15 February 2017
Accepted 15 February 2017
Available online 24 February 2017

ABSTRACT

In the present work, the effect of the CaO/P_2O_5 ratio on the composition of sol-gel synthesized $58SiO_2$-$(19 - x)P_2O_5$–$(23 + x)$CaO (x = 0, 5, 10 and 15 mol%) glass samples was studied. Further, the effect of NBO/BO ratio on hydroxy carbonated apatite layer (HCA) forming ability based on dissolution behavior in simulated body fluid (SBF) solution was also investigated. CaO/P_2O_5 ratios of synthesized glass samples were 1.2, 2, 3.6, and 9.5, respectively. NBO/BO ratios were obtained using Raman spectroscopic analysis as 0.58, 1.20, 1.46, and 1.78, respectively. All samples were soaked in the SBF solution for 7 days. The calculated weight losses

* Corresponding author.
E-mail address: sr.kirankumarsr@gmail.com (P. Kiran).
Peer review under responsibility of Cairo University.

Production and hosting by Elsevier

http://dx.doi.org/10.1016/j.jare.2017.02.001

Keywords:
Sol-gel
Ca/P ratio
NBO/BO ratio
Dissolution
SBF solution
HCA layer

of these samples were 58%, 64%, 83%, and 89% for corresponding NBO/BO ratios. The increase in CaO/P_2O_5 ratio increases the NBO/BO ratios. However, the increase in NBO/BO ratio increases HCA forming ability of SBF treated samples. The HCA crystalline layer formation was confirmed through X-ray Diffraction (XRD), Transmission Electron Microscopy (TEM), Scanning Electron Microscopy (SEM), Raman and Infrared spectroscopic analysis. Higher CaO/P_2O_5 ratio favors the increase in HCA formation for SBF treated calcium phospho silicate glasses.

Introduction

SiO_2-CaO-P_2O_5 based glasses constitute a promising material for bioactive applications for bone repair, tissue regeneration in the human body, etc. [1]. Implantation of these materials in the human body induces a specific biological response at the material interface and can promote new bone formation without forming fibrous tissues. This new bone can form a bond to living bone inside the human body [2]. The bone bonding ability of these materials has been attributed to the deposition and growth of a hydroxyapatite (HA) layer, which is close to bone mineral composition [3]. In crystallization process, HA layer can get converted as hydroxy carbonated apatite (HCA) layer in the presence of SBF solution [4].

Sol-gel technique is an alternative route to synthesize the bioactive glasses with higher purity and homogeneity in comparison with conventional melt quenching technique [5–8]. Compared to the melt quenching method, sol-gel method enables obtaining the glasses with higher porosity and surface area to improve bone bonding rates and excellent resorption and degradation in physiological environments [2,9,10]. The limitation of SiO_2 content to get HA layer for SBF soaked calcium phosphosilicate glasses is 60 mol% in melt quenching method and 90 mol% in sol-gel method. Due to this reason, the sol-gel method is the best feasible technique to get a HA layer formation compared to melt quenching method [11–14].

HCA layer formation in the presence of SBF solution for glasses depends on different process parameters such as glass composition [15], porosity [11], preparation method [16], precursors [6], and sintering temperature [17]. In bio-medical applications, HCA formation in SBF solution mainly depends on the dissolution behavior of the glass matrix [18]. In dissolution process, glass network connectivity is one of the interesting factors [6]. In the case of calcium phosphosilicate glasses, SiO_2 and P_2O_5 are network formers. The commonly used network modifiers such as CaO and Na_2O release cations of Ca^{2+}, Na^+ which migrate into SBF solution. This process eventually leads to the disconnectivity of the glass network and results in the formation of silanol groups. Later, it can affect the formation of silica gel layer through the polycondensation process, which acts as an implanted material for HCA formation [19].

In the case of CaO-P_2O_5-SiO_2 gels, increase in SiO_2 content increases the crystalline intensities of β and γ-($Ca(PO_3)_2$) phases [20]. Laczka et al. [21] reported that gel polymerization and crystallization process at different temperature conditions depend on the selection of precursors for CaO and P_2O_5 contents. Sopcak et al. [22] reported the precipitation mechanism for CaO-SiO_2-P_2O_5 system depends on different Ca/P ratios at different pH values, and also revealed that increase in calcium content increases amorphous nature.

For SiO_2-CaO glasses HCA forming ability in SBF solution depends on the ratio of sample weight to volume of SBF solution in incubation conditions [5]. For SiO_2-CaO-P_2O_5 glasses, the studies related to the improvement in the HCA growth rate in SBF solution are available based on precursors used in the synthesis process and heat-treatment conditions [2]. According to Ahsan and Mortuza [23], the addition of P_2O_5 up to 5 mol% can depolymerize the glass system. In calcium phosphosilicate glasses, orthophosphate units depolymerize the glass system and can also play the same role as Na_2O, i.e., network modifier [21]. Sun et al. [24] reported that the increase in P_2O_5 composition (P_2O_5 > 9%) can enhance the degree of polymerization by acting as a network former [25].

In this work, $58SiO_2$-$(19 - x)P_2O_5$–$(23 + x)$CaO [x = 0, 5, 10 and 15 mol%] glasses have been synthesized using the sol-gel method. These glasses were soaked in the SBF solution for 7 days to get HCA formation on the glass surface. Thermal, structural and morphological properties were studied using X-ray Diffraction (XRD) technique, Thermo Gravimetric Analysis with Differential Thermal Analysis (TGA/DTA) and Scanning Electron Microscopy with Energy Dispersive X-ray (SEM/EDX) Analysis. Raman, Fourier Transmission Infrared (FTIR), and Transmission Electron Microscopy with Selected Area Energy Dispersive (TEM/SAED) techniques were performed on these glasses. Notably, the NBO/BO ratio effect on HCA forming ability studies for SiO_2-CaO-P_2O_5 bioactive glass system in SBF solution, is not adequate. In the present study, NBO/BO ratio was found using Raman spectroscopic analysis. The impact of CaO/P_2O_5 content on NBO/BO ratio and the effect of NBO/BO ratio on HCA forming ability for SBF soaked glass samples were studied in detail.

Experimental

$58SiO_2$-$(19 - x)P_2O_5$–$(23 + x)$ CaO [x = 0, 5, 10 and 15 mol%] glasses were synthesized by conventional sol-gel process and samples were named as SCP1, SCP2, SCP3, and SCP4, respectively, as shown in Table 1. Chemicals for synthesis were purchased from Merck company (Mumbai, India). The precursors used for the preparation of these glasses were tetraethylorthosilicate [$Si(OC_2H_5)_4$], triethylphosphate (TEP) [$(C_2H_5O)_3PO$], calcium nitrate tetrahydrate [$Ca(NO_3)_2{\cdot}4H_2O$]. Further, H_2O, 2 N of HNO_3 were selected as solvents [(mol of H_2O)/(mol of TEOS + mol of TEP) = 10] and [(mol of HNO_3)/(mol of TEOS + mol of TEP) = 0.05], respectively. Tetraethylorthosilicate (TEOS) was mixed with H_2O, HNO_3 and stirred for one hour. At an interval of one-hour TEP, calcium nitrate was added subsequently and the solution was stirred well. The prepared sols were poured into Teflon beakers, sealed with aluminum wrappers and kept in hot air oven at 60 °C for three days of aging and subsequently the aged gels were dried at 130 °C for 4 h. The dried gels were ground, made into powder and heated at a rate of 5 °C/min up to 700 °C and stabilized at that temperature for 4 h to obtain glass samples in the powder form. After getting powder samples, pellets have been prepared using a hydraulic press by applying 5 tons of pressure for 5 min [26].

The SBF solution was prepared by dissolving KH_2PO_4, $CaCl_2$, $NaHCO_3$, $MgCl_26H_2O$, KCl and NaCl in deionized water (at pH = 7. 4) with Tris-buffer, by maintaining the temperature at 37 °C [1]. The pelletized SCP samples were soaked in SBF solution on the basis of sample surface area/SBF solution volume ratio as 8 mm^2/mL.

Characterization

The glass transition temperature (T_g) and onset crystalline temperature (T_x) were identified by the TGA and DTA analysis (SII EXTRAR 6000, Japan) with a flow rate of 10 °C/min in the temperature range

Table 1 TGA/DTA measurements for $58SiO_2$-$(19 - x)P_2O_5$–$(23 + x)$CaO glasses.

x mol%	Glass sample name	SiO_2 (mol%)	P_2O_5 (mol%)	CaO (mol%)	First weight loss (°C)	Second weight loss (°C)	T_g (°C)	T_x (°C)
0	SCP1	58	19	23	452	554	402 ± 0.19	723 ± 0.20
5	SCP2	58	14	28	488	545	479 ± 0.28	764 ± 0.13
10	SCP3	58	9	33	494	558	415 ± 0.07	726 ± 0.09
15	SCP4	58	4	38	494	563	481 ± .0.15	774 ± 0.15

27–1000 °C. Weight loss of samples, before and after SBF treatment was measured using an electronic weighing balance [Sartorius, BT224s, India]. The structural properties of all samples have been investigated using the Powder X-ray Diffractometer (Rigaku, Miniplux 600, Japan) with a scan rate of 2°/min.

Spherical shaped HA crystalline nuclei of SCP samples were observed by TEM/SAED (JEOL JEM 2100, Japan), SEM (JEOL_JSM-6380LA, Japan) and elements present in the samples were identified by the EDX analyzer (JEOL, Japan). The types of chemical bands were identified by the FTIR spectrometer (SHIMADZU-8400s, North America). For FTIR analysis, the pellets were prepared using 300 mg of KBr mixed with 1 mg quantity of stabilized and SBF treated SCP glasses. The pellets were analyzed in the wave number range between 400 and 1800 cm^{-1} at a rate of 25 scans/min with the resolution of 4 cm^{-1}. Room temperature Raman spectroscopy was performed using a LABRAM-HR800 (Japan). To avoid laser heating of the samples, the incident power was kept at a low value of 2 mW. The pH value of SBF solution was measured using pH meter (Eutech, pH 510, India) before and after soaking SCP samples. Ca^{2+} and PO_4^{3-} ion concentrations were measured using Flame Photometer (ELICO CL378, Germany) and UV/Vis absorption spectrometer (HITACHI PM & E 101, Canada).

Results and discussion

TGA/DTA analysis

Thermal behavior SCP samples were studied using TGA/DTA analysis and the results are shown in Fig. 1(a–d). Two weight losses (T_{WL1} and T_{WL2}) were observed for SCP samples at different temperature conditions using TGA curves. The first weight loss (WL1) was observed at 452–494 °C related to the evaporation of organics (alkoxy groups) [26–27]. The second weight loss (WL2) related to the thermal evaporation of residual nitrates has been observed at 545–563 °C [26–28]. Glass transition (T_g) temperature and crystalline onset temperature (T_x) values were measured three times using the DTA curves for SCP dried gels as shown in Table 1. The glassy forming ability is naturally related to the crystalline phase itself. The variations in T_g and T_x values are related to the change of the primary crystalline phase.

Lucas-Girot et al. [29] and Letaïef et al. [30] reported that for low P_2O_5 content, phosphorous is not considered as a glass former like silicon and it is present in the glass structure as PO_4^{3-} ions like a glass modifier. Aguiar et al. [31] observed that, to get HA formation for SiO_2-P_2O_5-CaO-Na_2O-MgO glasses, phosphorous does not act as a network former. Silicate glasses enhance the bioactivity with inclusion of a small P_2O_5 amount. This remarkable inversion in the effect of P_2O_5 would be explained in the following way. Some of the phosphorous forms P-O-Si links and reduces the bioactivity (considered as negative effect) and some other is found as free orthophosphate, whose relatively fast initial release accelerates the HA deposition and boosts the bioactive process (considered as positive effect). The balance between these opposite effects decides the bioactivity of the P-containing composition. Based on the bioactivity data of the compositions modeled, Tilocca and Cormack [32] concluded that the negative effect prevails for high P_2O_5 fractions, whereas positive effect prevails for that lower (below 10 mol% P_2O_5) fractions. From these literature supports, it could be concluded that P_2O_5 acts as a network former for SCP1 and SCP2 samples in the present study (with > 10 mol% P_2O_5). For SCP3 and SCP4 samples P_2O_5 acts as a network modifier (with < 10 mol% P_2O_5).

T_g and T_x values vary with P_2O_5 content. As the (x) mol% increases from 0 to 5%, the T_g and T_x values increase. The observed P_2O_5 quantity is greater than 10 mol% in SCP1 and SCP2 samples and in this case, it (P_2O_5) acts as network former. P_2O_5 content is higher for SCP1 compared to SCP2 sample. Network former addition polymerizes the silicate network and decreases the required temperature to get glass formation as reported in the literature [24,28]. As the P_2O_5 content is changing from 5 to 9 mol%, it acts as a network modifier. Compared to SCP2, SCP3 sample has less polymerization effect. In the network modifier case polymerization reduces and it leads to decrease in T_g and T_x values. As the mol% increases from 10 to 15% the T_g and T_x values increase. SCP3 and SCP4 samples have P_2O_5 less than 10 mol%. In this case, P_2O_5 acts as a network modifier and changes in T_g and T_x values depending on network modifier concentrations. Carta et al. [7] reported that increase in network modifier content increases T_g and T_x values for soda lime phosphosilicate glasses. CaO (network modifier) content is more in SCP4 than SCP3 sample and P_2O_5 also acts as a network modifier for these samples. Depending on the network modifiers, increase in glass transition temperature and crystalline onset temperature takes place [25]. There is no significant weight loss above 700 °C in TGA curves. DTA curves show exothermic peaks above 700 °C. Due to this reason, 700 °C is considered as a stabilization temperature for SCP samples [27,28,33].

XRD analysis

The XRD pattern of SCP samples is shown in Fig. 2(a). The XRD pattern has broadband between the diffracted angles 20°–30°, indicating the amorphous nature. This occurs due to the internal disorders and glassy nature of the materials sintered at 700 °C. It was also confirmed by DTA analysis. The SBF treated samples show the crystalline nature [as shown in Fig. 2(b)]. The dominant HA crystallite peak was identified at $2\theta = 32°$ [$(hkl) = (211)$] corresponding to $Ca_5(PO_4)_3(OH)$ [HA] (JCPDS 01-074-0565). Calcite phase also was observed at $2\theta = 29°$ (JCPDS NO 01-081-2027) [27,34]. Another HA peak was observed at 38°. The intensities of three major reflections (211), (300), and (002) increased from SCP1 to SCP4 sample.

During SBF treatment, a chemical reaction takes place on the sample surface. In this process calcium, phosphate ions migrate into SBF solution and form silanol groups. Due to polycondensation process silica gel layer forms on the sample surface. Calcium and phosphate ions migrate through silica gel layer and form calcium phosphate (apatite) layer on the sample surface. Due to crystallization process between apatite layer and existed calcium, phosphate, hydroxyl ions in SBF solution, hydroxyapatite (HA) layer forms on the sample surface [6,11]. HA layer growth depends on Ca^{2+} and PO_4^{3-} ion dissolution of the sample. Lower P_2O_5 content favors formation of more orthophosphate (PO_4^{3-}) units in the sample. Increase in CaO and decrease in P_2O_5 contents increase the Ca^{2+} and PO_4^{3-} ions which are released into SBF solution. This further leads to increase in HA layer formation on the sample surface [33]. Due to this reason, the HA crystalline intensities have increased from SCP1 to SCP4 sample. CaO/P_2O_5 ratios for SCP1 to SCP4 samples are 1.2, 2, 3.6, and 9.5, respectively. From these observations, it can be confirmed that increase in CaO/P_2O_5 ratio increases the HA crystallinity for SBF treated samples.

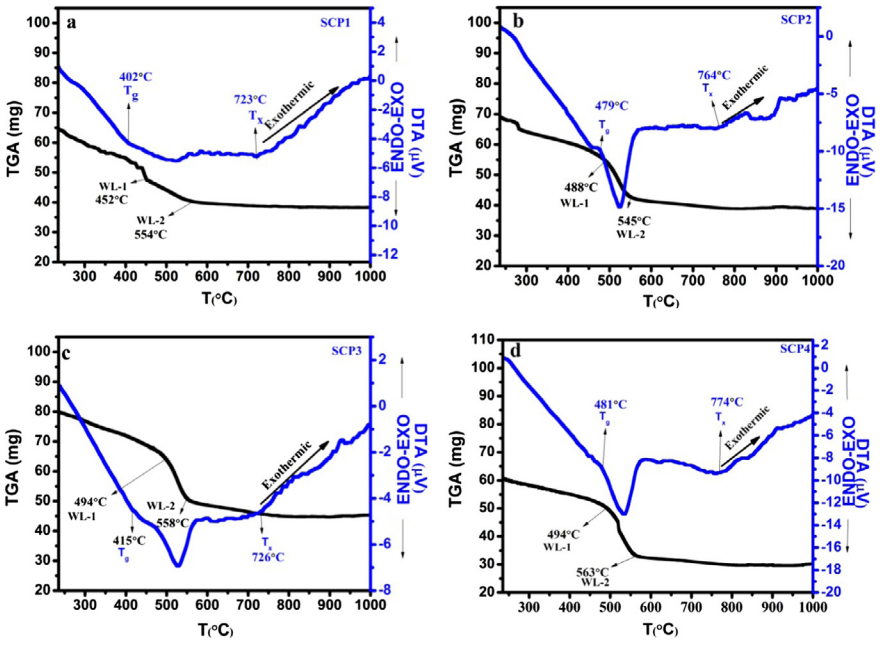

Fig. 1 TGA/DTA curves of (a) SCP1, (b) SCP2, (c) SCP3 and (d) SCP4 dried gels at 130 °C.

HA formation is increased from SCP1 to SCP4 sample. Formed HA consumes Ca^{2+} ions and getting released into SBF solution, it leads to decrease in Ca^{2+} ion concentration in SBF solution and forms $CaCO_3$ layer due to a chemical reaction between calcium and carbonate ions [18]. Due to this reason, calcite crystalline peak intensities have decreased from SCP1 to SCP2 samples (In this case P_2O_5 acts as network former).

The calcite intensities were increased from SCP2 to SCP3 sample, since the polymerization effect is more in SCP2 than SCP3 sample (in the case of SCP3, P_2O_5 acts as network modifier). The number of Ca^{2+} ions released by SCP2 samples is less and these Ca^{2+} ions react with PO_4^{3-} ions and form HA layer. Dissolution of Ca^{2+} and PO_4^{3-} ions is more in SCP3 sample and forms HA layer with less Ca^{2+} ions expense of SBF. Calcite intensities were decreased from SCP3 to SCP4 sample, since formed HA consumes more Ca^{2+} ions.

Surface morphology

The surface morphology of SCP samples before and after SBF treatment is shown in Fig. 3. For SBF untreated SCP samples EDX analysis confirmed that elements present in the samples are Si, Ca, P and O as shown in Fig. 3(a, e, i and m). SBF untreated samples have a homogeneous surface morphology [Fig. 3(b, f, j and n)]. For SBF treated samples, the surface morphology [Fig. 3(c, g, k and o)] clearly exhibits the spherical shaped HCA nuclei formation on the sample surface. It is observed that the lower P_2O_5 concentration (increase in CaO) leads to increase in HCA nuclei progressively on the glass surface. For SBF treated samples, the EDX analysis of HCA layer has shown the presence of Ca, P, C and O elements on the sample surface [Fig. 3(d, h, l and p)]. The increase in Ca and P intensities of these samples indicates the increase in HA layer formation on the sample surface. In the previous section, it has been discussed that the crystallization process between apatite and existed calcium, phosphate and hydroxyl ions leads to HA formation on the sample surface. In this process, with CO_3^{2-} presence, HA layer gets converted into as HCA layer [6].

All SBF treated samples show good homogeneity in particle size with the relevant HCA particle size distributions. HCA nuclei average sizes were increased for SCP1 to SCP4 samples as from 821 nm to 1259 nm. It indicates that the average particle sizes of HCA nuclei have increased with increase in CaO/P_2O_5 ratio, and similar studies have been reported in the literature [35]. SCP samples consist of CaO content in the increasing order from SCP1 to SCP4 samples. The increase in CaO content increases Ca^{2+} ions release into SBF solution and it leads to increase in HA layer formation on the sample surface. EDX analysis shows that Ca and P intensities [related to HA] increased from SCP1 to SCP4 sample.

Raman analysis

For SCP samples Si-O-Si asymmetric stretching (as s) and Si-O-NBO asymmetric stretching (as s) modes were assigned at 1027–1080 cm^{-1} and 961–967 cm^{-1} wave number regions, respectively, as shown in

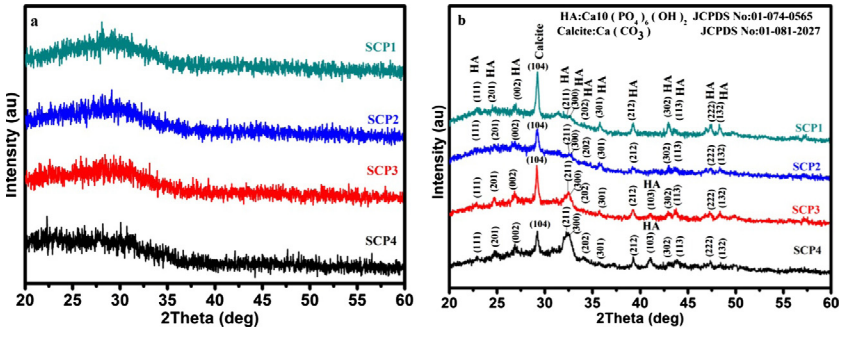

Fig. 2 XRD pattern of SCP glass samples (a) before, (b) after soaking in SBF solution.

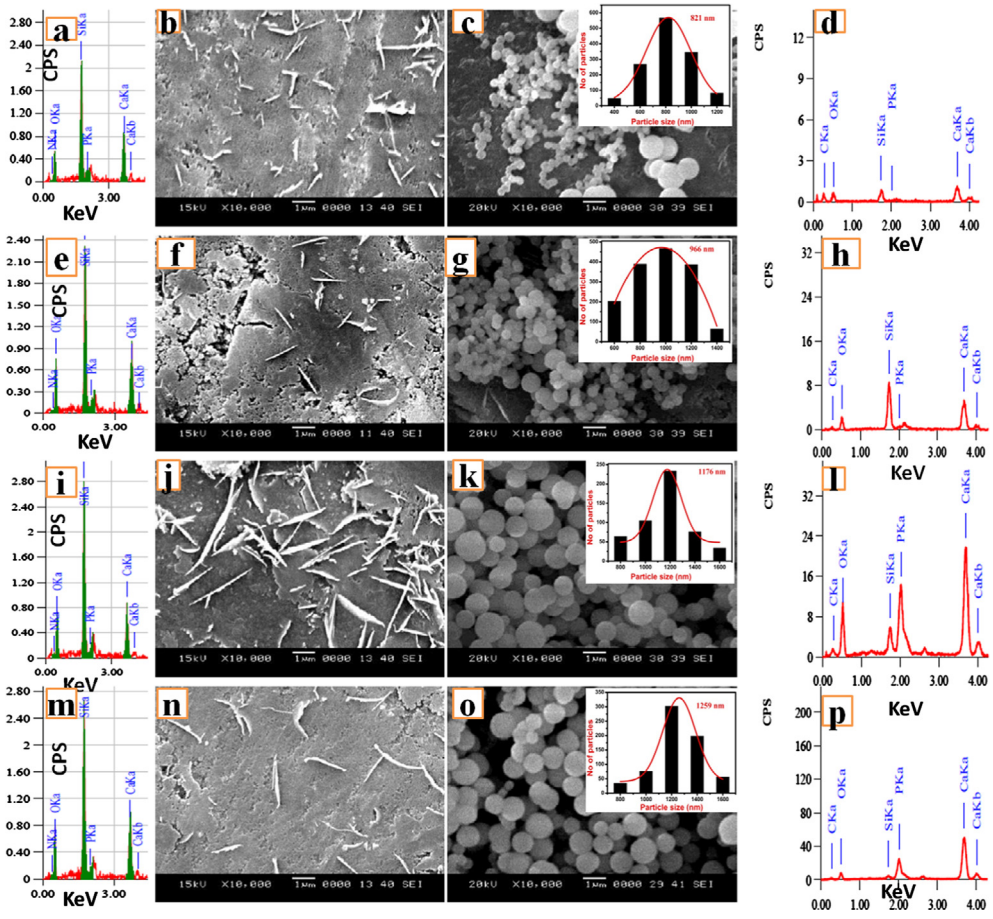

Fig. 3 (a, e, i and m) EDX analysis, (b, f, j and n) SEM images of SBF untreated SCP1, SCP2, SCP3 and SCP4 samples. (c, g, k and o) SEM images with particle size distribution, (d, h, l and p) EDX analysis of SBF treated SCP1, SCP2, SCP3 and SCP4 samples.

Fig. 4(a) [Table 2]. Fivefold symmetric stretching [W_1] modes were also observed at 460–477 cm^{-1}. For the identification of NBO modes in silicate tetrahedra, the deconvolution process has been used in the wave number range of 800–1200 cm^{-1} [Fig. 4(b–e)]. Si-O-NBO (as s) intensity/Si-O-BO (as s) intensity [NBO/BO] ratios have been obtained using deconvolution process. The deconvolution curve fittings were considered based on the fitting curve area is proportional to band intensities [36]. The obtained NBO/BO ratios of SCP1, SCP2, SCP3 and SCP4 samples are 0.58, 1.20, 1.46, and 1.78, respectively. Increase in CaO/P_2O_5 ratio increases NBO/BO ratio and increase in NBO/BO ratio decreases the degree of polymerization between silicate and phosphate tetrahedra. The electronegativity of Si^{4+} is predominated by the electronegativity of P^{5+} ion for SCP1 and SCP2 glasses. Due to this, NBOs of silicate tetrahedra convert as that of phosphate tetrahedra. Repolymerization takes place between silicate and phosphate tetrahedra. Decrease in P_2O_5 decreases the polymerization, and it leads to increase in the T_g, T_x values from SCP1 to SCP2 glass. SCP3 and SCP4 glasses have less P_2O_5 compared to SCP1 and SCP2 glasses, and in this case electronegativity of Si^{4+} predominates the electronegativity of P^{5+} ion. The NBO conversion from silica tetrahedra to phosphate tetrahedra is very less for SCP3 compared to SCP2 sample, and in this case phosphate phases form as clusters. Compared to SCP2, in SCP3 sample Phosphate phase size (cluster size) is more. O'Donnell et al. [37] reported that increase in Phosphate phase size decreases the T_g and T_x values. Due to this reason T_g and T_x values were decreased from SCP2 to SCP3 glass. In the case of SCP3 and SCP4 samples, decrease in P_2O_5 content decreases the phosphate phase size. SCP4 sample has less P_2O_5 compared to SCP3 sample, and due to this reason phosphate phase size decreases in SCP4 compared to SCP3 sample. Ca^{2+} ion effect is also more for SCP4 compared to SCP3 sample, and it causes the increase in T_g and T_x values for SCP4 compared to SCP3 sample.

For SBF treated samples CO_3^{2-} asymmetric stretching modes appeared in the wave number range of 1084–1086 cm^{-1} as shown in Raman spectra [Fig. 4(f)]. PO_4^{3-} symmetric stretching modes were also observed at 954–965 cm^{-1} wave number region. For SCP4 samples HA related crystalline PO_4^{3-} bending modes and fivefold symmetric stretching [W_1] modes were also observed at 591 cm^{-1} and 433 cm^{-1}, respectively [Table 2]. Crystalline intensities of CO_3^{2-} modes increased from SCP1 to SCP4 sample. Due to this reason HCA formation also increases for SCP samples, and also that the HCA growth is carbonates depended [38].

FTIR analysis

FTIR spectroscopic analysis of SCP samples is shown in Fig. 5(a). The transition bands observed at 1064–1187 cm^{-1} were assigned to the Si-O-Si asymmetric stretching (as s) and Si-O-NBO (as s) modes were assigned at 1026–1033 cm^{-1}. For SCP samples, different intensities occur at 466–478 cm^{-1} related to rocking modes of Si-O-Si [Table 3]. Si-O-Si bending modes were observed in the wave number region of 779–794 cm^{-1}. PO_4^{3-} asymmetric stretching modes of vibrations are also observed at 1222–1265 cm^{-1}. The decrease in P_2O_5 content decreases the degree of polymerization between silicate and phosphate tetrahedra, and due to this reason phosphate tetrahedra have less prominence and silicate tetrahedra have more prominence supported by the literature [33].

For SBF treated samples [Fig. 5(b)] Si-O-Si asymmetric stretching mode became broader compared to SBF untreated samples in the FTIR spectra (1022–1087 cm^{-1}), and this is due to the formation of silica gel (amorphous) layer on the sample surface in the dissolution

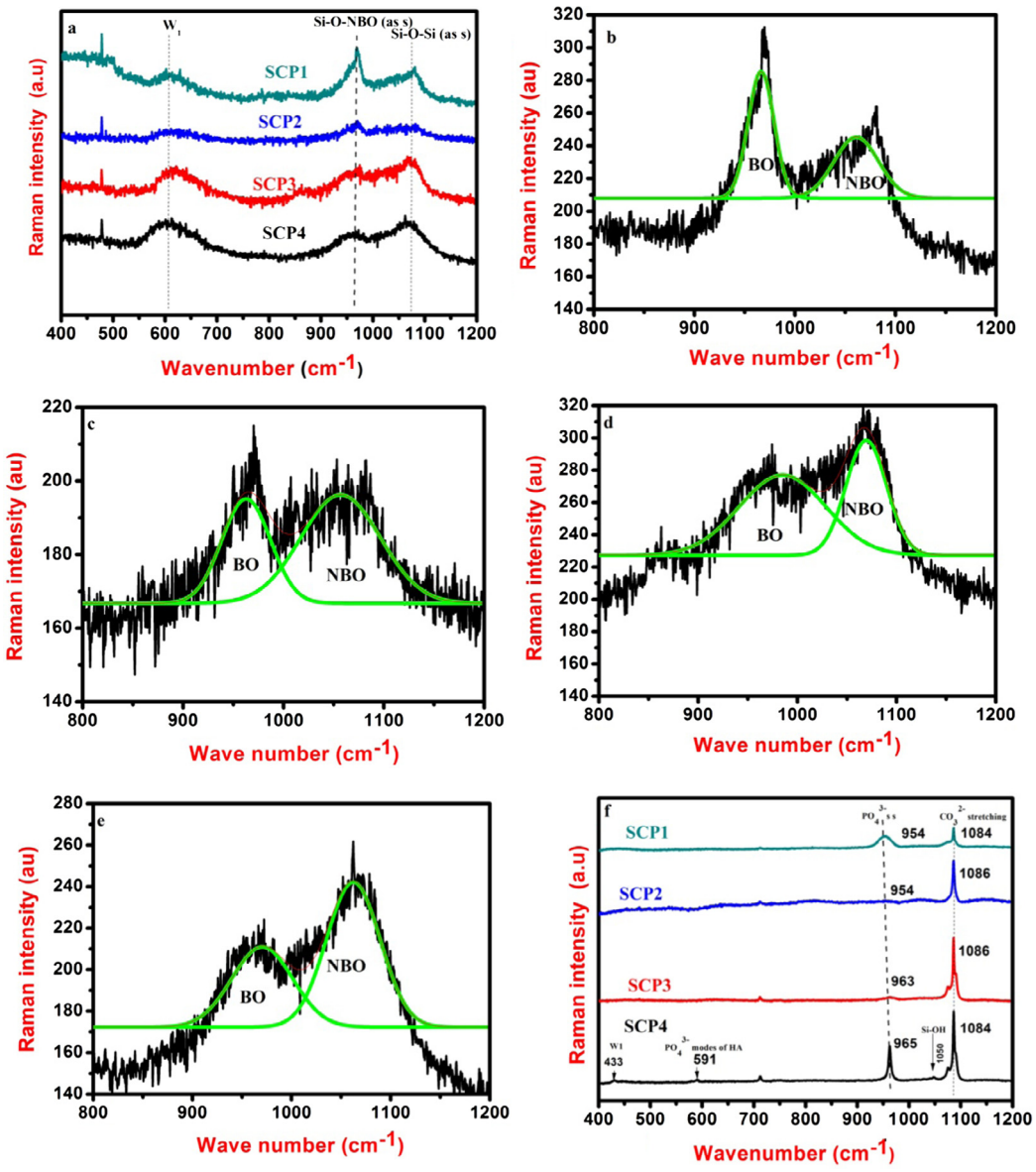

Fig. 4 (a) Raman spectra of SCP samples before SBF treatment, (b), (c), (d) and (e) are deconvoluted Raman spectra of SCP1, SCP2, SCP3 and SCP4 samples respectively. (f) Raman spectra of SCP samples after SBF treatment.

process. For SBF treated samples CO_3^{2-} bending (1413–1498 cm^{-1}) modes became broader and more prominent compared to SBF untreated samples. Sharp, intense CO_3^{2-} stretching modes (~873 cm^{-1}) were also observed for SBF treated samples compared to SBF untreated samples [Table 3]. For SBF treated samples PO_4^{3-} bending amorphous mode (601–605 cm^{-1}) broadness was decreased and sharpness was increased compared to SBF untreated samples. The increase in sharpness is related to the formation of PO_4^{3-} bending crystalline modes which are assigned at 669 cm^{-1}.

From these observations, it can be concluded that during the crystallization process the HCA crystalline layer would be formed in the presence of carbonate groups. XRD, SEM/EDX and Raman spectroscopic analysis confirmed the HCA crystal formation on the sample surface in dissolution process.

It is also observed that the OH groups are also present in the FTIR spectra before and after SBF treatment at 1635–1643 cm^{-1} and 1641 cm^{-1} wave number regions, respectively. It may be due to absorbed water from the environment during the pelletization process [39]. Si-O-Si rocking, bending modes were present in the wave number range of 464–470 cm^{-1} and 785–794 cm^{-1}, respectively after SBF treatment. Non-Bridging oxygen modes related to Si-O-Ca were also observed for SBF treated SCP3 and SCP4 samples at 923–925 cm^{-1}.

TEM/SAED analysis

The TEM analysis revealed that SBF treated samples have spherical shaped particles as shown in Fig. 5(c–f). The d-spaces [for (211) plane] for spherical shaped particles are found using TEM/SAED pattern [40]. The observed d-spaces for SCP1, SCP2, SCP3, and SCP4 samples are 0.280 nm, 0.283 nm, 0.279 nm, and 0.281 nm, respectively. The observed $d_{(211)}$-spaces are in good agreement with standard JCPDS (24-0033) files of HCA layer. From these observations, it can be concluded that for SBF treated samples the formed crystals are HCA particles in the dissolution process.

pH assessment, dissolution and weight loss studies

In dissolution process, calcium and phosphate ions migrate into SBF solution, forming silanol groups on the sample surface. In

Table 2 Raman band assignments of Calcium phosphosilicate glasses before and after soaking in SBF solution [38–41].

Before soaking in SBF solution					After soaking in SBF solution				
SCP1	SCP2	SCP3	SCP4	Assigned bands	SCP1	SCP2	SCP3	SCP4	Assigned bands
Raman absorption band in cm^{-1}									
463	471	477	460	W1	–	–	–	433	W1
961	967	966	965	Si-O-NBO asymmetric stretching	–	–	–	591	PO_4^{3-} Modes of HA
1073	1027	1080	1076	Si-O-Si asymmetric stretching	954	954	963	965	PO_4^{3-} symmetric stretching
					–	–	–	1050	Si-OH
					1084	1086	1086	1084	CO_3^{2-} stretching

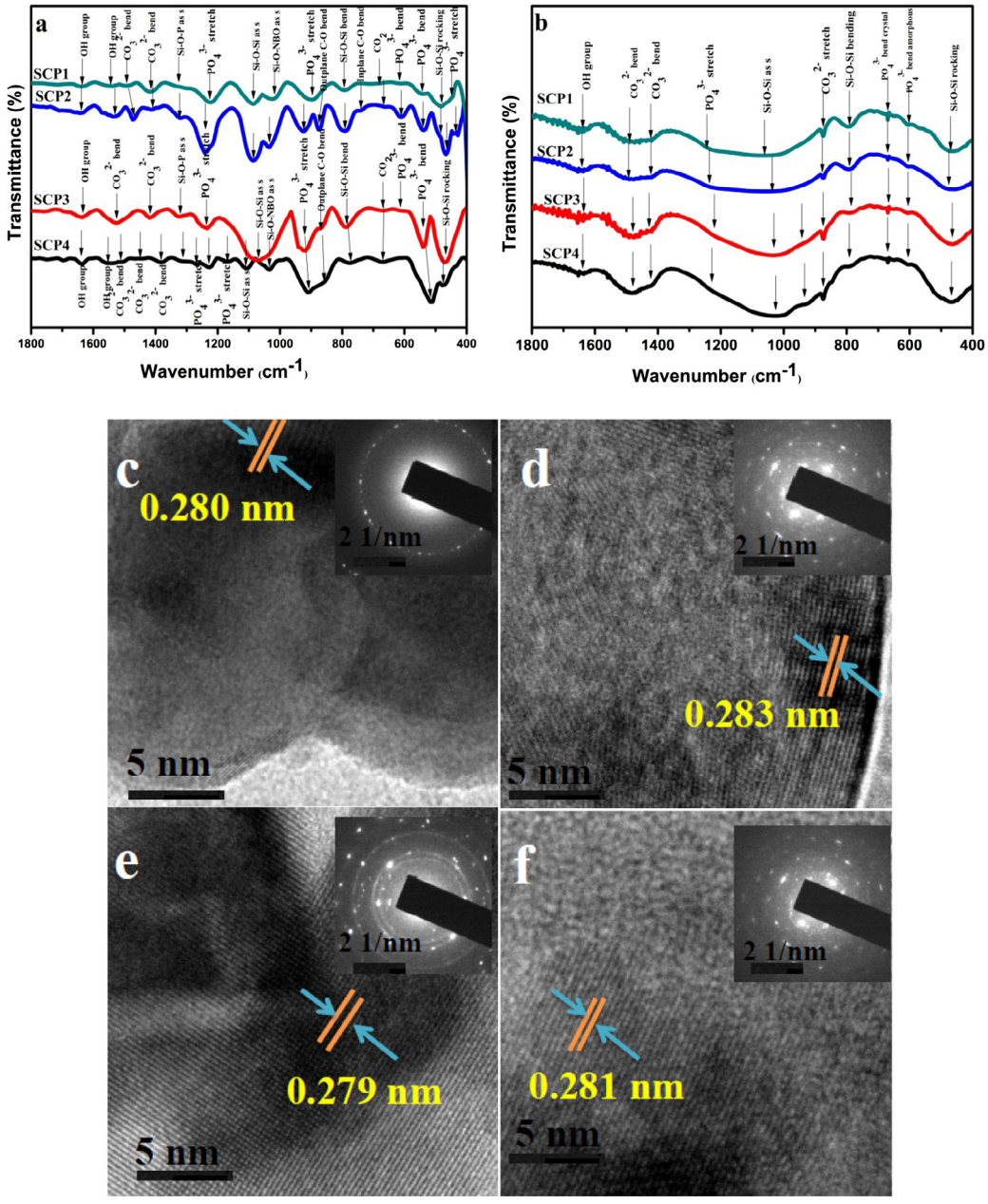

Fig. 5 (a), (b) FTIR spectra of SCP samples before and after SBF treatment. (c), (d), (e), and (f) TEM/SAED analysis of SBF treated SCP1, SCP2, SCP3, and SCP4 samples.

polycondensation process silanol groups form silica gel layer on the sample surface. Calcium and phosphate ions of glass matrix leach on the silica gel layer surface as amorphous calcium phosphate (apatite) layer, and it changes the Ca^{2+} and PO_4^{3-} concentrations of SBF solution. Incorporation of Ca^{2+} and PO_4^{3-}, and hydroxyl and carbonate ions from SBF solution into apatite layer lead to

Table 3 FTIR band assignments of Calcium phosphosilicate glasses before and after soaking in SBF solution.

Before soaking in SBF solution						After soaking in SBF solution					
SCP1	SCP2	SCP3	SCP4	Assigned bands	References	SCP1	SCP2	SCP3	SCP4	Assigned bands	References
Infrared transition band in cm^{-1}											
445	429	–	–	PO_4^{3-} (as s)	[41]	468	470	464	466	Si-O-Si rocking	[43]
474	466	470	478	Si-O-Si rocking	[43]	601	605	603	601	PO_4^{3-} bending amorphous	[18]
536	540	540	516	PO_4^{3-} bending amorphous	[18]	669	669	669	669	PO_4^{3-} bending crystalline	[18]
613	609	617	–	PO_4^{3-} bending crystalline	[18]	794	792	792	785	Si-O-Si bending	[24]
677	663	671	671	CO_2	[31]	875	873	873	873	CO_3^{2-} stretching	[42]
794	790	786	779	Si-O-Si bending	[24]	–	–	925	923	Si-O-Ca (as s)	[31]
–	875	864	850	Out plane C-O bending	[40]	1078	1087	1035	1022	Si-O-Si (as s)	[24]
898	925	925	910	PO_4^{3-} (as s)	[24]	1228	1236	1214	1228	PO_4^{3-} (as s)	[42]
1026	1033	1033	1033	Si-O-NBO (as s)	[31]	1419, 1498	1419, 1498	1413, 1481	1434, 1494	CO_3^{2-} bending	[24]
1083	1187	1064	1103, 1172	Si-O-Si (as s)	[43]	1641	1641	1641	1641	–OH group	[44,45]
1222	1242	1234	1226,1265	PO_4^{3-} (as s)	[43]						
1334	1319	1326	1311	Si-O-P (as s)	[43,45]						
1415,1492	1411, 1472	1419, 1527	1380, 1465, 1512	CO_3^{2-} bending	[43]						
1639	1643	1635	1635	–OH group	[44,45]						

HCA formation on the sample surface in the crystallization process [6].

The pH values are increased up to 24 h of soaking time in the SBF solution as shown in Fig. 6(a). At this stage, due to the fast release of Ca^{2+} ions silanol groups have formed and it leads to the HA formation on the sample surface [18,27]. The pH values are almost stabilized after 24 h. The pH values, Ca^{2+} and PO_4^{3-} ion concentrations of SBF solution are increased [as shown in Table 4] from SCP1 to SCP4 samples as shown in Fig. 6(b) and (c). The weight loss of SBF treated SCP samples is also increased from SCP1 to SCP4 samples [Fig. 6(d)].

Raman and FTIR spectroscopy analysis of SCP samples revealed that the non-bridging oxygens exist as Si-O-Ca asymmetric stretching modes. The Raman spectroscopic analysis also revealed that NBO/BO ratio is increased for SCP samples with an increase in CaO/P_2O_5 ratio.

The Ca^{2+} and PO_4^{3-} ions release from glass matrix in the SBF solution depending on the Ca^{2+} and PO_4^{3-} ions in the glass matrix and degree of polymerization also. In the case of SCP1 and SCP2 samples, P_2O_5 acts as network former. Polymerization takes place between phosphate and silicate tetrahedra. P_2O_5 content is more and polymerization effect is also more for SCP1 than SCP2 sample, and due to this reason SCP2 sample releases more PO_4^{3-} ions than SCP1 sample. NBO/BO ratio is more for SCP2 sample than SCP1 sample and NBOs are in Si-O-Ca form. Due to low polymerization and higher NBOs, the Ca^{2+} release also increased from SCP1 to SCP2 sample. SCP3 and SCP4 samples have less P_2O_5 content, and in this case P_2O_5 acts as network modifier. Due to this reason polymerization effect is less for SCP3 and SCP4 samples, and orthophosphate units form as clusters with very weak P-O bands [37]. Phosphate phase cluster size (with orthophosphate units) is less for SCP4 compared to SCP3 sample. Due to this reason, SCP4 glass can release more PO_4^{3-} ions than SCP3 sample. Due to increase in NBO/BO ratio, Ca^{2+} ion release also increases from SCP3 to SCP4 sample. From all these observations it can be concluded that the Ca^{2+} and PO_4^{3-} ion release from glass matrix in the SBF solution increases from SCP1 to SCP4 sample. The increase in NBO/BO ratio increases the dissolution of Ca^{2+} ions into SBF solution, and it causes the increase in pH values of the SBF solution in the dissolution process for SCP samples.

In dissolution process, HA layer formation on the sample surface not only depends on number of releasing Ca^{2+} and PO_4^{3-} ions from the sample, but also on the number of leaching Ca^{2+} and PO_4^{3-} ions from SBF solution. The increase in the Ca^{2+} ion release depends on an increase in NBO/BO ratio. The decrement in glassy nature is based on P_2O_5 content for SCP1 to SCP4 samples and it results in the increase in the dissolving PO_4^{3-} ions. The increase in weight loss of SBF treated samples [Table 5] in the dissolution process occurs from SCP1 to SCP4 samples based on the increment in number of dissolution of Ca^{2+} and PO_4^{3-} ions from the sample into SBF solution.

Conclusions

$58SiO_2$-$(19 - x)P_2O_5$–$(23 + x)CaO$ (x = 0, 5, 10 and 15 mol%) glass samples were synthesized using conventional sol-gel method. In this work, the role of CaO/P_2O_5 content on NBO/BO ratio for synthesized glass samples and HA forming ability for SBF treated samples for 7 days were studied. The calcium phosphosilicate glasses were sintered at 700 °C. It was observed from TGA/DTA analysis that the glass transition and onset crystalline temperatures increase with an increase in CaO/P_2O_5 ratio. From the XRD analysis, it was confirmed that the samples sintered at 700 °C have shown the amorphous nature. The SBF treated samples for 7 days have exhibited crystalline nature. This crystalline nature indicates the HA forming ability. Surface morphology confirmed that the SBF treated samples have shown HCA nuclei formation on the sample surface and this formation increases with increase in CaO/P_2O_5 ratio. Raman spectroscopic analysis revealed that the increase in CaO/P_2O_5 ratio increases NBO/BO ratio. This study also identified carbonate and symmetric stretching phosphate groups in HCA layer. FTIR studies confirmed that the PO_4^{3-} bending crystalline modes are related to HA layer. This study also identified the carbonate and asymmetric stretching phosphate groups

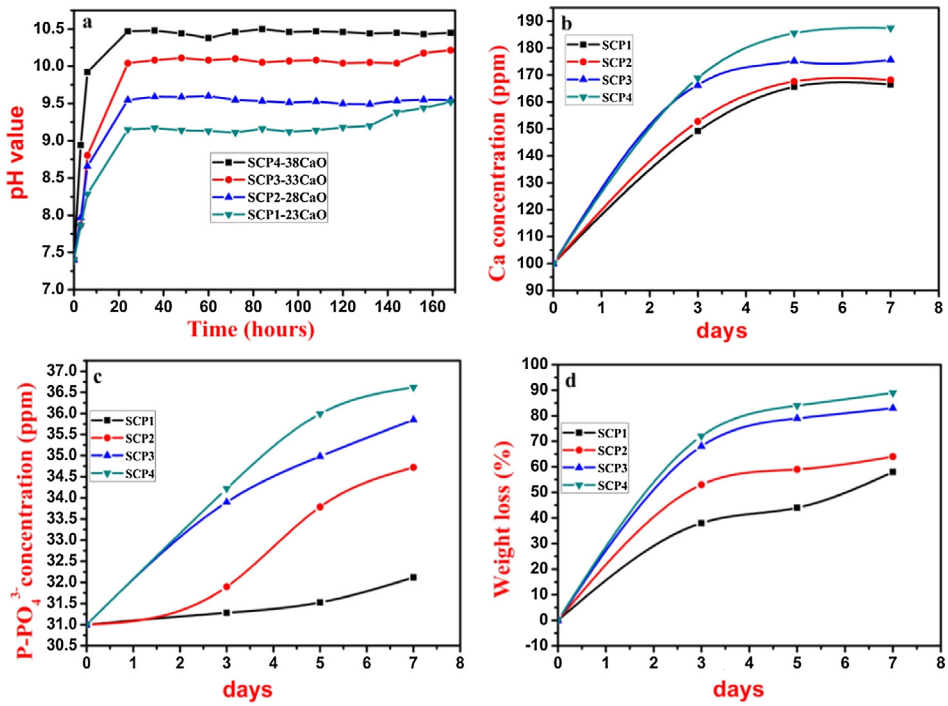

Fig. 6 (a) pH variation, (b) Ca concentration variation, (c) P concentration variation of SBF solution for SBF soaked SCP glasses with respect to soaking time and (d) Weight loss% variation of SBF soaked SCP glasses with respect to soaking time.

Table 4 PO_4^{3-}, Ca^{2+} ion concentration of SBF solution for $58SiO_2$-$(19 - x)P_2O_5$–$(23 + x)CaO$ glasses in ppm.

	PO_4^{3-} ion concentration (ppm)				Ca^{2+} ion concentration (ppm)			
Soaking time in SBF (days)	SCP1	SCP2	SCP3	SCP4	SCP1	SCP2	SCP3	SCP4
0	31	31	31	31	100	100	100	100
3	31.28	31.89	33.89	34.21	149.2	152.8	166.2	168.9
5	31.52	33.78	34.98	35.99	165.6	167.6	175.1	185.6
7	32.12	34.71	35.84	36.62	166.5	168.2	175.6	187.5

Table 5 HCA nuclei sizes, $d_{(211)}$-space of HCA and Weight loss % of SBF soaked $58SiO_2$-$(19 - x)P_2O_5$–$(23 + x)CaO$ glasses with NBO/BO ratio.

x mol%	NBO/BO ratio Raman	Nuclei average size (nm) SEM	$d_{(211)}$ (nm) TEM/SAED	Weight loss for SBF soaked samples (%)
0	0.58	821	0.280	58
5	1.20	966	0.283	64
10	1.46	1176	0.279	83
15	1.78	1259	0.281	89

in HCA layer. The Ca^{2+} and PO_4^{3-} ion release from glass matrix in the SBF solution is increased from SCP1 to SCP4 sample. Due to this reason there occurs weight loss of the samples in the dissolution process. TEM/SAED analysis confirmed that those formed crystals are HCA crystals in the dissolution process. This work supports the controlling hard tissue (bone) regeneration rates based on CaO/P_2O_5 ratio in glass system.

Conflict of Interest

The authors have declared no conflict of interest.

Compliance with Ethics Requirements

This article does not contain any studies with human or animal subjects.

Acknowledgments

The authors gratefully acknowledge to the National Institute of Technology Karnataka, Surathkal-575025, India, for providing research facilities and financial support. The authors are also thankful to Mrs. Thrithila Shetti for providing ion release test facilities and fruitful discussion.

References

[1] Kokubo T, Takadama H. How useful is SBF in predicting *in vivo* bone bioactivity? Biomater 2006;27:2907–15.
[2] Bellucci D, Sola A, Salvatori R, Anesi A, Chiarini L, Cannillo V. sol-gel derived bioactive glasses with low tendency to crystallize:

synthesis, post-sintering bioactivity and possible application for the production of porous scaffolds. Mater Sci Eng C 2014;43:573–86.
[3] Bellucci D, Sola A, Gazzarri M, Chiellini F, Cannillo V. A new hydroxyapatite-based biocomposite for bone replacement. Mater Sci Eng C 2013;33:1091–101.
[4] Yousefi A-M, Oudadesse H, Akbarzadeh R, Wers E, Lucas-Girot A. Physical and biological characteristics of nanohydroxyapatite and bioactive glasses used for bone tissue engineering. Nanotechnol Rev 2014;3:527–52.
[5] Shelby JE. Introduction to glass science and technology. Royal Society of Chemistry; 2005.
[6] Jones R, Clare AG. Bio-glasses an introduction. A John Wiley & Sons, Ltd., Publication; 2012.
[7] Carta D, Knowles JC, Smith ME, Newport RJ. Synthesis and structural characterization of P_2O_5–CaO–Na_2O sol–gel materials. J Non-Cryst Solids 2007;353:1141–9.
[8] Catauro M, Dell'Era A, Ciprioti SV. Synthesis, structural, spectroscopic and thermoanalytical study of sol-gel derived SiO_2-CaO-P_2O_5 gel and ceramic materials. Thermochim Acta 2016;625:20–7.
[9] Goller G, Oktar FN, Ozyegin LS, Kayali ES, Demirkesen E. Plasma-sprayed human bone-derived hydroxyapatite coatings: effective and reliable. Mater Lett 2004;58:2599–604.
[10] Arcos D, Vallet-Regí M. Sol–gel silica-based biomaterials and bone tissue regeneration. Acta Biomater 2010;6:2874–88.
[11] Wu C, Chang J. Mesoporous bioactive glasses: structure characteristics, drug/growth factor delivery and bone regeneration application. Interface Focus 2012;2:292–306.
[12] Siqueira RL, Zanotto ED. The influence of phosphorus precursors on the synthesis and bioactivity of SiO_2–CaO–P_2O_5 sol–gel glasses and glass–ceramics. J Mater Sci Mater Med 2013;24:365–79.
[13] Radev L. Influence of thermal treatment on the structure and *in vitro* bioactivity of sol-gel prepared CaO-SiO_2-P_2O_5 glass-ceramics. Process Appl Ceram 2014;8:155–66.
[14] Catauro M, Bollino F, Papale F, Mozetic P, Rainer A, Trombetta M. Biological response of human mesenchymal stromal cells to titanium grade 4 implants coated with PCL/ZrO hybrid materials synthesized by sol-gel route:*in vitro* evaluation. Mater Sci Eng C 2014;45:395–401.
[15] Zhang L, Gou Z. Incorporation of B_2O_3 in CaO-SiO_2-P_2O_5 bioactive glass system for improving strength of low-temperature co-fired porous glass ceramics. J Non-Cryst Solids 2012;358:1171–9.
[16] Liu W, Wu X, Zhan H, Yan F. Synthesis of bioactive poly (ethylene glycol)/SiO_2-CaO-P_2O_5 hybrids for bone regeneration. Mater Sci Eng C 2012;32:707–11.
[17] Hashmi MU, Shah SA, Umer F, Alkedy AS. Effect of sintering temperature on microstructure and *in vitro* behavior of bioactive glass-ceramics. Ceram-Silik 2013;57:313–8.
[18] Peitl O, Dutra Zanotto E, Hench LL. Highly bioactive P_2O_5-Na_2O-CaO-SiO_2 glass-ceramics. J Non-Cryst Solids 2001;292:115–26.
[19] Lukito D, Xue JM, Wang J. *In vitro* bioactivity assessment of 70 (wt.)% SiO_2-30 (wt.)% CaO bioactive glasses in simulated body fluid. Mater Lett 2005;59:3267–71.
[20] Sooraj Hussain N, Lopes MA, Santos JD. A comparative study of CaO–P_2O_5–SiO_2 gels prepared by a sol–gel method. Mater Chem Phys 2004;88:5–8.
[21] Laczka M, Cholewa-Kowalska K, Kulgawczyk K, Klisch M, Mozgawa W. Structural examinations of gel-derived materials of the CaO-P_2O_5-SiO_2 system. J Mol Struct 1999;511:223–31.
[22] Sopcak T, Medvecky L, Girman V, Durisin J. Mechanism of precipitation and phase composition of CaO-SiO_2-P_2O_5 systems synthesized by sol–gel method. J Non-Cryst Solids 2015;415:16–23.
[23] Ahsan MR, Mortuza MG. Infrared spectra of $xCaO(1-x-z)SiO_2$ zP_2O_5 glasses. J Non-Cryst Solids 2005;351:2333–40.
[24] Sun Y, Zhang Z, Liu L, Wang X. FTIR, Raman and NMR investigation of CaO-SiO_2-P_2O_5 and CaO-SiO_2-TiO_2-P_2O_5 glasses. J Non-Cryst Solids 2015;420:26–33.
[25] Simon V, Mocuta H. Glass formation and dissolution properties Of Na_2O-CaO-P_2O_5 glasses in simulated body fluids. Rom Rep Phys 2004;56:424–9.
[26] Ma J, Chen CZ, Wang DG, Hu JH. Synthesis, characterization and *in vitro* bioactivity of magnesium-doped sol–gel glass and glass-ceramics. Ceram Int 2011;37:1637–44.
[27] Masoud M, Fatholla M, Mohammadreza T. Investigation of physic-chemical reactivity of a mesoporous bioactive SiO_2-CaO-P_2O_5 glass in simulated body fluid. J Non-Cryst Solids 2010;356:1470–8.
[28] Yang X, Zhang L, Chen X, Sun X, Yang G, Guo X, et al. Incorporation of B_2O_3 in CaO -SiO_2-P_2O_5 bioactive glass system for improving strength of low-temperature co-fired porous glass ceramics. J Non-Cryst Solids 2012;358:1171–9.
[29] Lucas-Girot A, Fatima ZM, Mohamed M, Hassane O, Abdelhamid H, Marie LF. Sol-gel synthesis of a new composition of bioactive glass in the quaternary system SiO_2-CaO-Na_2O- P_2O_5 comparison with melting method. J Non-Cryst Solids 2011;357:3322–7.
[30] Letaïef N, Lucas-Girot A, Oudadesse H, Dorbez-Sridi R, Boullay P. Investigation of the surfactant type effect on characteristics and bioactivity of new mesoporous bioactive glass in the ternary system SiO_2-CaO-P_2O_5: structural, textural and reactivity studies. Micropor Mesopor Mater 2014;195:102–11.
[31] Aguiar H, Solla EL, Serra J, González P, León B, Almeida N, et al. Orthophosphate nanostructures in SiO_2-P_2O_5-CaO-Na_2O-MgO bioactive glasses. J Non-Cryst Solids 2008;354:4075–80.
[32] Tilocca A, Cormack AN. Structural effect of phosphorous inclusion in bioactive silicate glasses. J Phys Chem B 2007;111, 14256-254.
[33] Singh RK, Kothiyal GP, Srinivasan A. *In vitro* evaluation of bioactivity of CaO-SiO_2-P_2O_5-Na_2O-Fe_2O_3 glasses. Appl Surf Sci 2009;255:6827–31.
[34] Ahmed A, Simon CFR, Robert GH. The role of MgO on thermal properties, structure and bioactivity of bioactive glass coating for dental implants. J Non-Cryst Solids 2012;358:3019–27.
[35] Zhao S, Li Y, Li D. Synthesis and *in vitro* bioactivity of CaO-SiO_2-P_2O_5 mesoporous microspheres. Micropor Mesopor Mater 2010;135:67–73.
[36] Marsich L, Moimas L, Sergo V, Schmid C. Raman spectroscopic study of bioactive silica-based glasses: the role of the alkali/alkali earth ratio on the Non-Bridging Oxygen/Bridging Oxygen (NBO/BO) ratio. J Spectrosc 2009;23:227–32.
[37] O'Donnell MD, Watts SJ, Law RV, Hill RG. Effect of P_2O_5 content in two series of soda lime phosphosilicate glasses on structure and properties-Part II: Physical properties. J Non-Cryst Solids 2012;358:3019–27.
[38] Rezwan K, Chen QZ, Blaker JJ, Boccaccini AR. Biodegradable and bioactive porous polymer/inorganic composite scaffolds for bone tissue engineering. Biomaterials 2006;27:3413–31.
[39] Bellucci D, Bolelli G, Cannillo V, Cattini, Sola A. *In situ* Raman spectroscopy investigation of bioactive glass reactivity: simulated body fluid vs Tris-buffered solution. Mater Charact 2011;62:1021–8.
[40] Lu W-H, Li K-D, Lu C-H, Teoh LG, Wu WH, Shen YC. Synthesis and characterization of mesoporous SiO_2–CaO–P_2O_5 bioactive glass by sol-gel process. Mater Trans 2013;54:791–5.
[41] Aguiar H, Serra J, González P, León B. Structural study of sol–gel silicate glasses by IR and Raman spectroscopies. J Non-Cryst Solids 2009;355:475–80.
[42] Notingher I, Boccaccini AR, Jones J, Maquet V, Hench LL. Application of Raman microspectroscopy to the characterisation of bioactive materials. Mater Charact 2002;49:255–60.
[43] Li HC, Wang DG, Hu JH, Chen CZ. Influence of fluoride additions on biological and mechanical properties of Na_2O-CaO-SiO_2-P_2O_5 glass–ceramics. Mater Sci Eng C 2014;35:171–8.
[44] Li HC, Wang DG, Hu JH, Chen CZ. Effect of various additives on microstructure, mechanical properties, and *in vitro* bioactivity of sodium oxide-calcium oxide-silica-phosphorus pentoxide glass–ceramics. J Colloid Interface Sci 2013;405:296–304.
[45] Inas B, Amany EIN. Physical properties of nano-composite silica-phosphate thin film prepared by sol-gel technique. New J Glass Ceram 2012;2:17–22.